JOURNAL OF AIRCRAFT
Vol. 43, No. 2, March–April 2006

Oscillating Wing Loadings with Trailing-Edge Strips

P. Gerontakos* and T. Lee†
McGill University, Montreal, Quebec H3A 2K6, Canada

The dynamic-load loops of an oscillating NACA 0012 airfoil, obtained from surface-pressure measurements, fitted with small full-span trailing-edge strips, positioned on the lower (i.e., the Gurney flaps) and/or upper (the inverted strips) surface at the wing trailing edge, of height of 1.6 and 3.2% of the airfoil chord were studied at $Re = 1.07 \times 10^5$. The results show that, similar to a static wing, the Gurney flap concept was also fairly generally applicable, in terms of lift performance enhancement, to an oscillating airfoil, despite the large and small increases in the peak negative pitching moment and maximum drag force, respectively, as well as a promoted dynamic stall. The increase (decrease) in the nose-down pitching moment (dynamic-stall angle) can be alleviated by the use of inverted strips at the price of a reduced maximum lift coefficient. The asymmetric strips were found to provide a compromise in the dynamic aerodynamic performance between the regular and inverted Gurney flaps, including a 49-deg flap, of an oscillating airfoil. The present passive oscillating-wing C_l-C_d-C_m control can be valuable, because it can be used as an experimental guideline for the active control of the dynamic stall and/or nose-down pitching moment via a spanwise trailing-edge flap.

Nomenclature

C_d	=	section pressure drag coefficient
C_l	=	section lift coefficient
$C_{l,\max}$	=	maximum lift coefficient
$C_{l\alpha}$	=	lift-curve slope, $dC_l/d\alpha$
C_m	=	section pitching-moment coefficient about $\frac{1}{4}$-chord
C_p	=	pressure coefficient, $(p - p_\infty)/\frac{1}{2}\rho u_\infty^2$
c	=	chord length without flap
f	=	oscillation frequency
h	=	flap or strip height
p	=	local static pressure
p_∞	=	freestream static pressure
Re	=	Reynolds number, cu_∞/ν
t	=	time
u_∞	=	freestream velocity
x	=	streamwise distance along the airfoil
y	=	transverse distance above the airfoil surface
α	=	angle of attack
α_{ds}	=	dynamic-stall angle
α_{LEV}	=	angle of attack at leading-edge-vortex formation
α_{ms}	=	moment-stall angle
α_{or}	=	angle of attack at onset of flow reattachment
α_{ss}	=	static-stall angle
α_0	=	zero-lift angle of attack
κ	=	reduced frequency, $\omega c/2u_\infty$
ν	=	fluid viscosity
ρ	=	fluid density
ω	=	angular frequency, $2\pi f$

I. Introduction

THROUGH their influence on the Kutta condition, the camber and geometry of the trailing edge of an airfoil can be used to manipulate the generation of lift and form drag, as well as the formation of the wake. Various types of trailing-edge flow separation control schemes have been studied by researchers elsewhere to maintain the high lift coefficient required, especially, for approach and landing and takeoff. One extensively studied device is the Gurney flap.

The Gurney flap is a simple device located at the trailing edge of the airfoil on the pressure side, perpendicular to the chord. It was originally used on the inverted wings of racing cars to increase the downforce and improve tire adherence for lateral traction required during high-speed turns. The idea behind this trailing-edge modification is to shift the location of the Kutta condition, thus enhancing the lift generated by the lifting surface at a given angle of attack. Liebeck[1] pioneered the experimental work of a Newman symmetric airfoil with a Gurney flap of 1.25% of the wing chord and reported a substantial increase in airfoil lift accompanied by a slight reduction in drag. The observed increase in the airfoil circulation and thus the lift is presumably associated with the downward turning of the flow near the trailing edge. A number of studies were later conducted,[2–14] and they further substantiate that, as occurs with other trailing-edge high-lift devices, the Gurney flap can significantly increase the lift, the maximum lift coefficient, and the lift-curve slope with small changes in the drag and the stalling incidence and that the optimum Gurney flap height scales with the boundary-layer thickness at the airfoil trailing edge. Also, the wake downstream of a Gurney flap consists of a von Kármán vortex sheet of alternately shed vortices.[11] No coherent wake structure was observed with the Gurney flap absent. The vortex shedding increases the suction at the trailing edge on the suction side of the airfoil; on the pressure side of the airfoil, the Gurney flap decelerates the flow and thus increases the pressure. The two changes result in a pressure difference acting across the trailing edge of an airfoil, which generates an increase in loadings and circulation over the whole of the airfoil. It is also observed that the performance of an airfoil with a 45-deg trailing-edge flap, or strip, is superior to the same airfoil with a similarly sized Gurney flap.[8]

In summary, the addition of a Gurney flap to a wing delays boundary-layer separation and yields an increase in the maximum lift coefficient. However, because of the drag and, especially, the nose-down pitching moment penalty caused by the Gurney flap, it would be desirable to conceal the flap during cruise in fixed-wing aircraft applications. Nonetheless, the high lift coefficients produced by a Gurney flap with minimum mechanical complexity and weight penalty have always provided a potential alternative for the design of mechanically simpler high-lift systems with no degradation in the aircraft performance for approach and landing and takeoff. Furthermore, knowing that Gurney flaps, or small trailing-edge strips, of a height comparable to the thickness of the boundary layer, could also render an increase in the lift-to-drag ratio and nose-down pitching moment, in addition to the substantially improved lift performance, it would be interesting to investigate their effects on the passive

Received 18 January 2005; revision received 4 April 2005; accepted for publication 6 April 2005.

*Graduate Research Assistant, Department of Mechanical Engineering.
†Associate Professor, Department of Mechanical Engineering. Member AIAA.

control of the undesired, or detrimental, hysteresis observed in the dynamic-load loops of an oscillating airfoil.

The phenomenon of dynamic stall and the accompanied high lift, pitching, and torsional loadings on oscillating or constant-pitching airfoils have been studied for many years, both as an important practical problem and as a challenging fundamental one as well. Dynamic stall generally occurs on helicopter retreating blades, which is a limiting factor for the high-speed performance of modern helicopters and on the rapidly pitched wings of supermaneuverable aircraft. This unsteady lift-enhancing mechanism has also been employed by insects to generate the large lift forces needed. Numerous experimental and computational investigations[15–19] have shown that the unsteady flow can be separating or reattaching over a large portion of the upper surface of the oscillating airfoil and that the predominant feature of the dynamic stall is the formation and rapid convection over the upper surface of the airfoil of an energetic leading-edge vortex (LEV), also referred to as the dynamic-stall vortex, which induces a nonlinearly fluctuating pressure field and produces large transient variations in forces and moments that are fundamentally different from their steady-state counterparts. The presence of a LEV leads to a delayed stall through the delay of large separation effects to increased angles of attack and enables the rapid generation of significant unsteady lift forces before any vorticity is shed. Note that there is a penalty, though, when a large LEV develops because there are large pressure gradients that result in large drag forces as well as lift forces. After the LEV begins convecting over the airfoil, there is a sudden decrease in pitching moment, and once the LEV passes the airfoil trailing edge and moves into the wake the flow progresses to a state of full separation over the upper surface, and an abrupt loss of lift is incurred. Subsequently, if and when the angle of attack becomes low enough during the pitch-down motion, the flow will finally reattach again from the leading edge. An excellent review on unsteady airfoils is given by McCroskey.[16]

The objective of the present study was to investigate the effects of small full-span trailing-edge strips on the dynamic-load C_l-C_d-C_m loops, determined by an integration of the surface-pressure distribution, of an oscillating NACA 0012 airfoil. Eight different trailing-edge strip configurations of two different heights, including a 49-deg flap and two asymmetric strips, were tested. The small strips were fitted normal to the local curvature on the lower and/or upper surface at the trailing edge of the wing model. Surface-pressure distributions of a static wing with and without the trailing-edge strips were also obtained for comparison.

II. Experimental Methods and Apparatus

The experiment was conducted in the recently constructed 0.9 m × 1.2 m × 2.7 m low-speed, suction-type wind tunnel at McGill University with a freestream turbulence intensity of 0.03% at $u_\infty = 35$ m/s. A NACA 0012 airfoil, fabricated from solid aluminum, with a chord length c of 15 cm and a span b of 37.5 cm, was used as the test model. The origin of the coordinate was located at the leading edge of the airfoil with x, y, and z in the streamwise, normal, and spanwise directions, respectively. The airfoil was fitted with two 30-cm-diam endplates with sharp leading edges to isolate the end effects. The gaps between the oscillating airfoil and the stationary endplates were kept at less than 1 mm to minimize the leakage of flow through the gaps. The two-dimensional uniformity of the flow distribution over the airfoil model was checked by traversing a 5-μm normal hot-wire probe located at 10%c downstream from the leading edge of the airfoil and $y = 5$ mm above the airfoil. The nonuniformity was found to be ±3% of the freestream value. The effect of the trailing-edge strip size was investigated by testing strip heights h of 1.6 and 3.2% chord with a thickness of 0.25% chord. The trailing-edge strip was fitted normal to the local curvature, on the lower [referred to as the Gurney flap (GF)] or upper [referred to as the inverted-trailing-edge strip (ITES)] surface at the trailing edge of the wing model. Two asymmetric strips formed by a combination of a 1.6%c ITES and a 3.2%c GF and a 3.2%c ITES and a 1.6%c GF, hereafter are referred to as 1.6%c/3.2%c and 3.2%c/1.6%c strips, respectively, as well as a 49-deg flap of $h/c = 3\%$, were also tested. The flaps were attached to the trailing edge by using double-sided Mylar adhesive film. The flap dimensions are given in Fig. 1. The chord Reynolds number was fixed at $Re = 1.07 \times 10^5$.

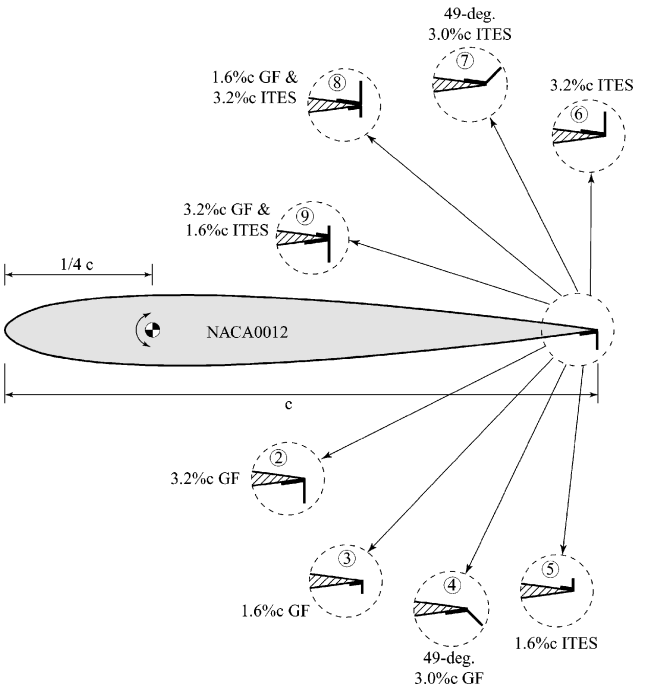

Fig. 1 Trailing-edge strip (TES) configuration. ITES denotes inverted TES and GF Gurney flap.

A specially designed four-bar linkage and flywheel oscillation mechanism, capable of oscillating the airfoil sinusoidally at various amplitudes and frequencies, was used in the present experiment. The mean angle of attack was varied by changing the relative angle between the rotating shaft and the rocker-shaft connector. The oscillation amplitude was varied by attaching the coupler at specific radial locations on the flywheel. A range of oscillation frequencies f (= 0.05 to 8.5 Hz) was obtained using a timing belt and pulley system attached to a variable-speed dc motor. The oscillation frequency was measured to an accuracy of ±0.02 Hz. The airfoil pitch axis was located at the $\frac{1}{4}$-chord location. The instantaneous angle of attack $\alpha(t)$ (=11 deg + 5 deg sin ωt, where $\omega = 2\pi f$ is the circular frequency, f is the oscillation frequency, and t is the time) of the airfoil and the phase reference signal $\tau = \omega t$ were recorded by using a potentiometer (TRW type DP 801) with an accuracy of ±0.1 deg. The airfoil was oscillated through the static-stall angle $\alpha_{ss} = 12.5$ deg with a reduced frequency κ ($= \omega c/2u_\infty$) of 0.05 and 0.1. Also, in the following discussion, the suffix u is used to indicate pitch-up when α is increasing and d is used to indicate pitch-down when α is decreasing.

The surface-pressure distributions were obtained from 61 0.35-mm-diam pressure taps, in conjunction with seven fast-response miniature pressure transducers (Type YQCH-250-1), distributed over the upper and lower surfaces along the midspan section of the wing model. The orifices were staggered 1.5 mm apart in the spanwise direction to avoid the wake effect from an upstream orifice on orifices further downstream. The pressure signals were phase-locked ensemble averaged over 100 cycles of oscillation and were integrated numerically to compute the unsteady aerodynamic loads and pitching moments. The dynamic range of the pressure transducer was on the order of 10 kHz. The transducer signals were low-pass filtered (250 Hz) and amplified with a multichannel AA Lab model G3006 pressure measurement system. The effects of the 18-cm-long and 0.75-mm i.d. plastic tubing, separating the surface tap and the pressure transducer, on the unsteady pressure signals were examined by comparing the transducer output level and the phase with a controlled acoustic sound source. The effect of the length of the plastic tubing was a simple time constant delay on all pressure signals with frequency above 2.95 Hz, which

rendered a limited reduced frequency κ of 0.126 at $u_\infty = 11$ m/s or $Re = 1.07 \times 10^5$ in the present experiment. Details of this method can be found in the work of Lee and Basu[18] and Rennie and Jumper.[20] For a static wing all surface pressures were scanned electronically through a 48-port scanivalve system. An uncertainty analysis gives a typical total uncertainty of ± 0.013 in C_p.

III. Results and Discussion

To facilitate the investigation of the trailing-edge strips on the dynamic-load loops of an oscillating wing, the variation of the C_l-C_d-C_m values of a static wing with and without trailing-edge strips was reexamined first and served as a reference for the unsteady airfoil results.

A. Static Wing

Figure 2a shows that for a static baseline wing a maximum lift coefficient $C_{l,\max}$ of 0.877 with a linear lift-curve slope $C_{l\alpha}$ $(= \mathrm{d}C_l/\mathrm{d}\alpha)$ of 0.0753 was obtained at a static-stall angle $\alpha_{ss} = 12.5$ deg. The stalling mechanism was of a sharp leading-edge stall type and was precipitated by bubble bursting. The existence of a laminar separation bubble was confirmed from the plateaus in the surface-pressure coefficient C_p distributions (up to $\alpha = 12.5$) in the leading-edge region of the airfoil (Figs. 3a–3c). For $\alpha > 12.5$ deg, the boundary layer completely separated from the leading edge and rendered a flat surface-pressure distribution (Fig. 3c). The nose-up pitching moment increased with low-to-moderate α; at α_{ss} the pitching moment experienced a sharp fall from positive to negative values with a peak negative pitching-moment coefficient $C_{m,\mathrm{peak}}$ of -0.0366 (Fig. 2c). A sharp rise in the drag coefficient C_d at α_{ss} was also observed (Fig. 2b). The drag polar presented in Fig. 2d also indicates that the baseline airfoil displayed a classical drag bucket with a rapid rise in lift-to-drag ratio (L/D) at $C_l = 0.15$ ($\alpha = 2$ deg) and was followed by a relatively flat L/D curve for low-to-moderate lift. At high C_l, the magnitude of L/D decreased with C_l and fell dramatically to values comparable to the low-C_l values for $\alpha > \alpha_{ss}$. A maximum lift-to-drag (C_l/C_d or L/D) ratio of 22.9 was observed at $\alpha = 6$ deg or $C_l = 0.52$.

The C_p distributions presented in Fig. 3a also show that with the addition of Gurney flaps (of $h/c = 1.6$ and 3.2%) the increased suction was evident everywhere on the upper surface while the lower surface experienced increased pressure. This resulted in a substantial increased lift coefficient with the GF, compared with the baseline configuration, as reported by researchers elsewhere. However, much of the lift increment was derived from a general increase in loading over the entire airfoil and a higher leading-edge suction peak (including the increase in the laminar-separation-bubble induced suction pressure; for example, see Fig. 3a), in addition to the observed increase in the aft loading of the airfoil. The increase in lift and pressure difference was most significant with a large GF and less profound with a small GF. The C_p distributions also indicate that at low incidences the Gurney flaps provided protection against a trailing-edge separation by reducing the pressure recovery demands (an effect comparable to the increase in dumping velocity caused by a conventional slotted flap[21]), which explains the longer linear portion in C_l-α curve (as shown in Fig. 2a). Above this incidence the Gurney flap promoted a localized suction pressure peak in the leading-edge region, pushing the boundary layer closer to separation and promoting the stalling mechanism. The stalling mechanism was, however, found to be similar to that of a baseline wing. The pressure distributions are incomplete (only covering up to 80% of the airfoil chord) because it is difficult to provide pressure tapping to the trailing-edge region of the 15-cm-chord airfoil model tested. The present static-wing results therefore somewhat underestimate the lift on the airfoil with flap. However, for an oscillating airfoil the aforementioned deficiency became less important because the

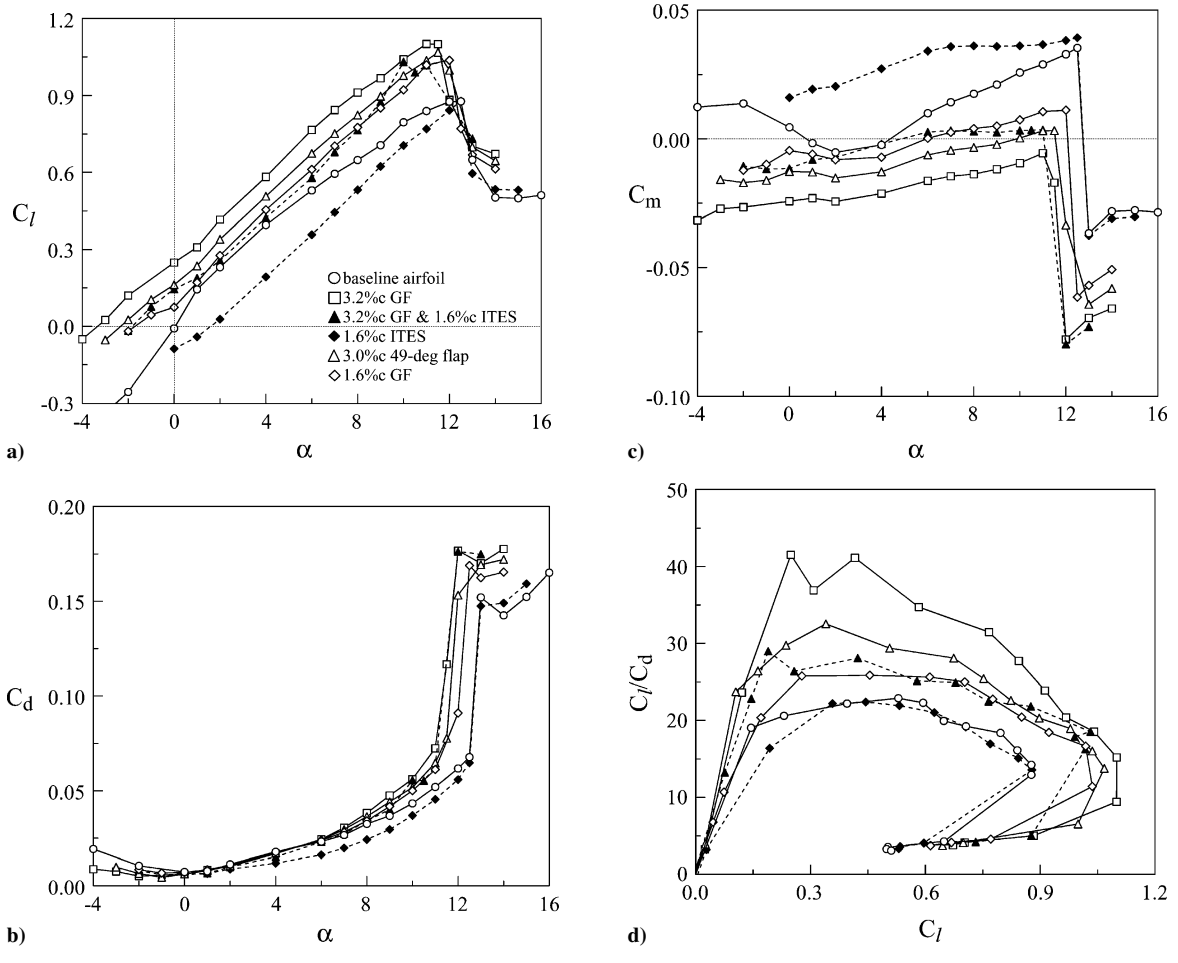

Fig. 2 Effect of trailing-edge strips on static-wing airloads.

Table 1 Variation of critical static aerodynamic performance with trailing-edge strip

Flap configuration	α_{ss}, deg	$C_{l,\max}$	$C_{l\alpha}$	α_0, deg	$C_{m,\text{peak}}$	L/D_{max}	$\alpha_{L/D_{max}}$ [a]	α_{ms}, deg[b]	$L/D_{\alpha ss}$ [c]
Baseline wing	12.5	0.877	0.0753	0	−0.0366	22.9	6	12.5	12.9
1.6%*c* GF	12.0	1.036	0.0848	−1.70	−0.0616	25.8	4	12.0	11.4
3.2%*c* GF	11.5	1.100	0.0815	−3.33	−0.0779	41.5	0	11.5	9.4
49-deg flap	11.5	1.067	0.0820	−2.32	−0.0644	32.5	2	11.5	13.7
1.6%*c* ITES	12.5	0.878	0.0813	1.60	−0.0376	22.4	7	12.5	13.6
1.6%*c* ITES + 3.2%*c* GF	11.0	1.031	0.0816	−1.82	−0.0799	29.0	1	11.0	16.4

[a] $\alpha_{L/Dmax}$ = airfoil incidence with L/D_{max}. [b] α_{ms} = moment stall angle. [c] $L/D_{\alpha ss}$ = L/D at α_{ss}.

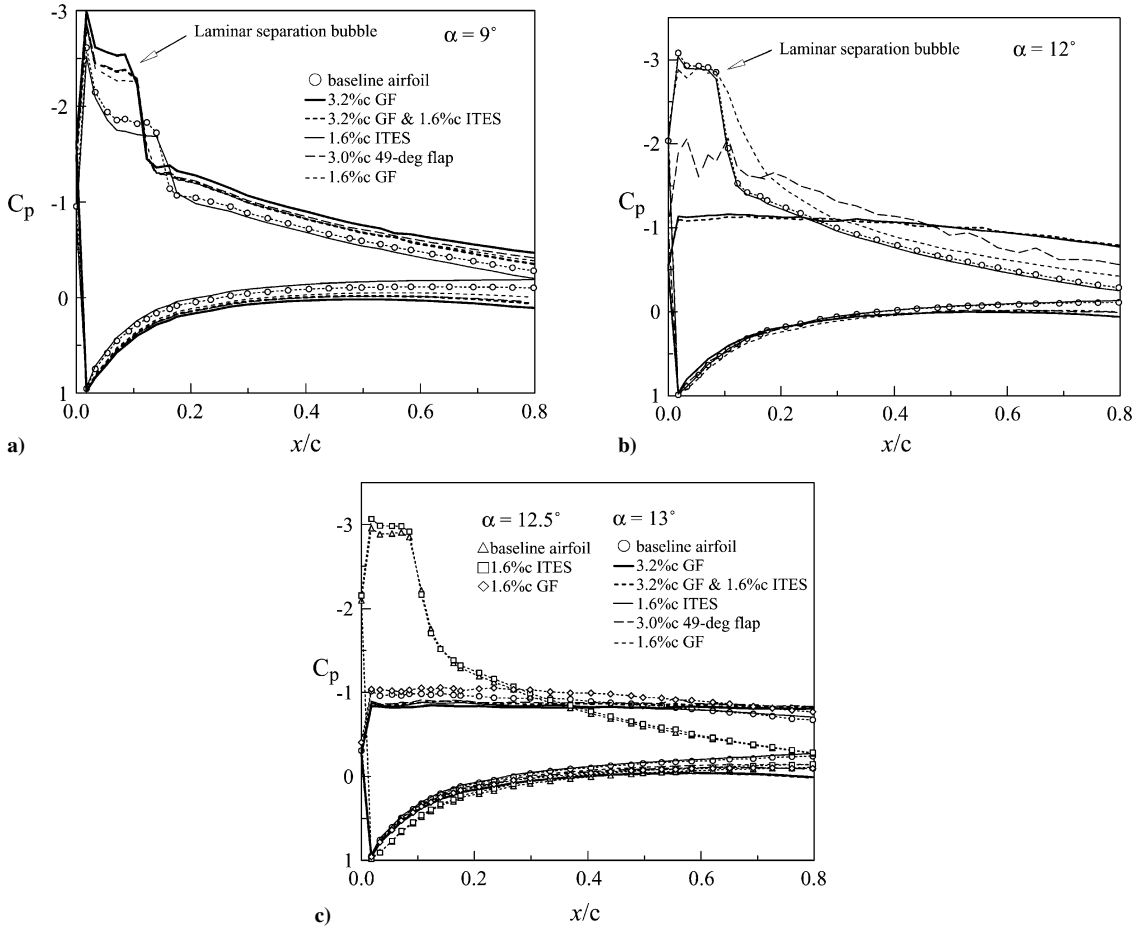

Fig. 3 Effect of trailing-edge strips on static-wing surface-pressure distributions.

unsteady boundary-layer flow and thus the dynamic lift is dominated by the formation, convection, and shedding of an energetic LEV formed in the leading-edge region of the airfoil.

Furthermore, comparison with the baseline wing shows that the lift curve was shifted upward and to the left with the Gurney flap (Fig. 2a). Consequently, the Gurney flap caused the angle of attack for zero lift α_0 to become increasingly more negative, suggesting that it served to increase the effective camber of the airfoil. The α_{ss} was decreased further as a larger GF was utilized. The addition of the Gurney flap, though, produced a significant lift increment in a linear fashion until stall for the symmetric airfoil, compared with the baseline configuration. The increase in lift obtained with the GF, however, came at the price of increasing drag (Fig. 2b) and negative pitching moments (Fig. 2c), which became more pronounced with increasing flap height. The results also show that with the flap the L/D curves were much wider in appearance compared with the baseline wing and were of higher value in L/D_{max} (Fig. 2d). The variation of the critical static aerodynamic performance with and without the flaps is summarized in Table 1.

The present measurements also indicate that a 49-deg flap also produced significant improvements in the airfoil performance. The pressure gradient over the wing upper surface was, however, milder than the 3.2%*c* GF (up to $\alpha < \alpha_{ss}$), but was superior to the smaller 1.6%*c* GF. Also, similar to the C_l, α_{ds} and L/D increment induced by the smaller GF tested, the 49-deg flap also served as a compromise in the alleviation of the undesirable increase in the nose-down pitching moment and C_d between the 3.2%*c* and 1.6%*c* flaps. Note also the rather gradual and unusual bubble disruption, especially the large fluctuations in C_p in the leading-edge region of the airfoil, at $\alpha = 12$ deg (Fig. 3b) of a 49-deg flap, compared to both the baseline and flapped wings. Detailed flowfield measurements are needed to explain the observed phenomenon.

Finally, the effects of inverted TES, including a 1.6%*c*/3.2%*c* asymmetric strip, on the critical aerodynamic performance were also examined. As expected, for a 1.6%*c* ITES, a decreased suction on the upper surface and pressure on the lower surface (in contrast to the GF), implying an upward turning of the flow, together with a significantly lowered leading-edge suction peak, which rendered a decreased lift performance, were observed. The ITES-induced negative camber effects shifted the lift curve vertically downward and led to an increased, or a positive, α_0 as well as a favorable nose-up pitching moment. There was a reduction in C_d up to the stall angle

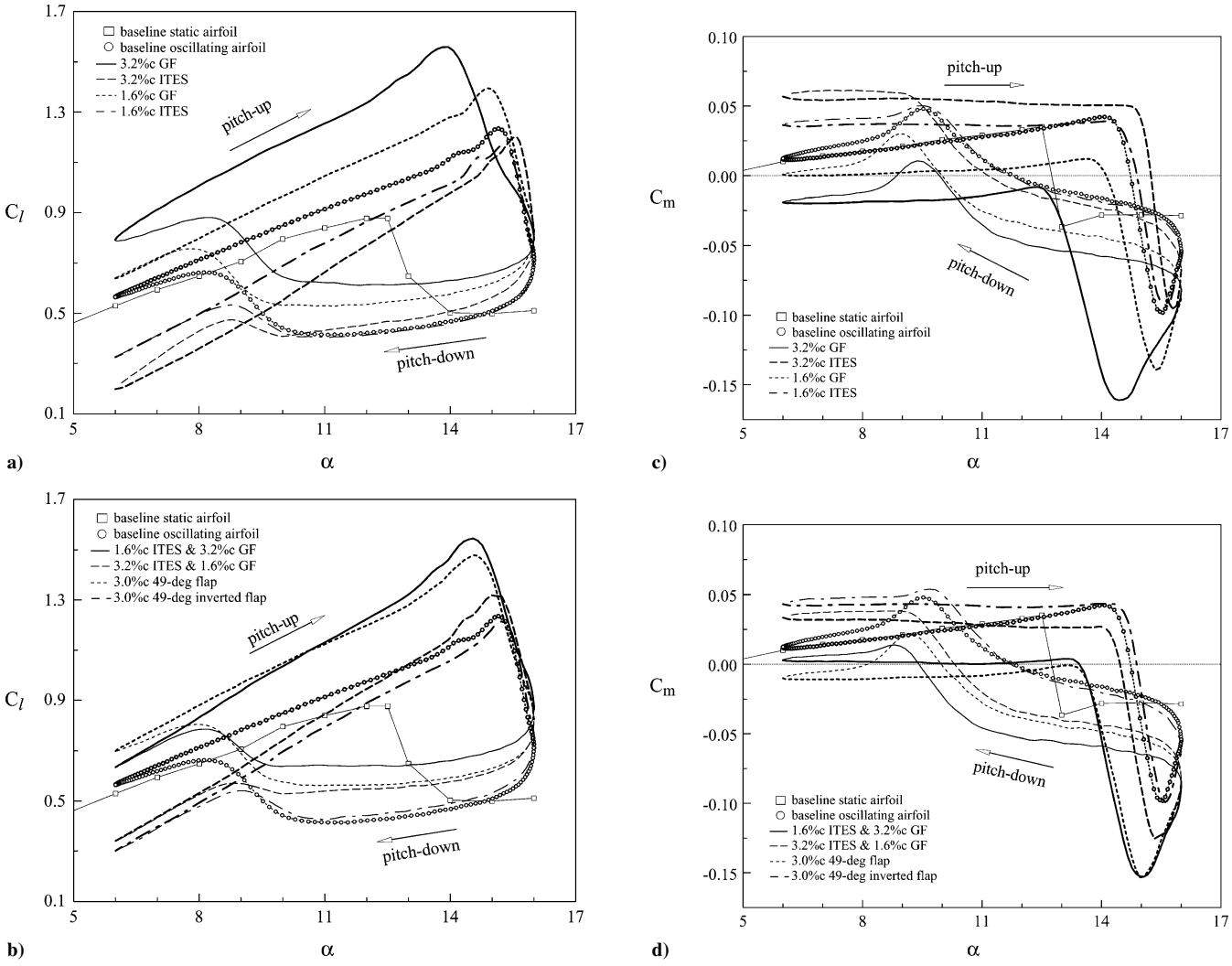

Fig. 4 Effect of trailing-edge strips on the dynamic load-loops for $\alpha(t) = 11$ deg + 5 deg sin ωt at $\kappa = 0.05$.

compared to a baseline wing. It is hypothesized that, in contrast to a GF, for a symmetric wing equipped with a small ITES the upward deflected stronger flow from the lower surface entrained and energized the weaker flow from the upper surface in the immediate wake downstream of the airfoil. The apparent consequence of this momentum transfer was, therefore, that the boundary-layer flow over the aft portion of the upper, suction surface was much less languid than the wing with and without a Gurney flap, thus reducing the wake width and drag. The stalling mechanism, though, remained unchanged (Fig. 3c). Furthermore, as a result of the lowered lift and drag coefficients, the L/D curve was found to be comparable to the wing without flap. On the other hand, the addition of a $1.6\%c/3.2\%c$ asymmetric strip was, in general, found to provide a compromise between a $3.2\%c$ GF and a $1.6\%c$ ITES.

B. Oscillating Wing

The phase-locked ensemble-averaged dynamic-load loops and surface-pressure distributions of a NACA 0012 airfoil oscillated with $\alpha(t) = 11$ deg $+ 5$ deg $\sin\omega t$ at $\kappa = 0.05$ with and without trailing-edge strips are presented in Figs. 4–7. Also shown in Fig. 4 are the static baseline wing data. The results show that for an airfoil oscillated beyond α_{ss} the unsteady boundary layer and stall events became more complicated, compared to its static counterparts. A large hysteresis in the dynamic-load loops, caused by the asymmetry between the flow separation and reattachment, is clearly seen (Fig. 4). The prior-to-stall flow condition was characterized by the presence and the upward spread of the flow reversal[19] (characterized by a thin layer at the bottom of the thickened turbulent boundary layer) and the subsequent formation, growth, and rapid downstream convection of an energetic LEV (Fig. 5), in contrast to the upstream propagation of the turbulent trailing-edge flow separation and the subsequent bubble bursting occurred on a static wing (as indicated in Fig. 3). The presence of a leading-edge laminar separation bubble and the formation (at $\alpha_u \approx 13.69$ deg), growth, and spillage (at $\alpha_u \approx 15.15$ deg) of a LEV on an oscillating baseline airfoil can be clearly identified from the plateau and the substantial rise and drop in the C_p distributions shown in Fig. 5. For an oscillating baseline airfoil, a 41.4% increase in $C_{l,\max} = 1.24$ at a dynamic stall angle $\alpha_{ds} = 15.15$ deg (Fig. 4a), compared to $C_{l,\max} = 0.877$ and $\alpha_{ss} = 12.5$ deg of a static baseline wing, mainly attributed to the boundary-layer improvement effects and, to a lesser extent, to the LEV transient effects (in contrast to the high-Reynolds-number results of Ericsson and Reding[15]), was observed. The dynamic lift stall, as a result of LEV spillage or detachment, was followed by a sudden collapse of lift (Fig. 4a) and was preceded by an abrupt drop in pitching moment as the LEV convected over the airfoil (Fig. 4c). The flow remained fully separated from the upper surface of the wing during the stall (Fig. 5). The poststall condition was characterized by a rather constant C_l (of a magnitude much lower than a static wing) for the most part of the pitch-down motion, followed by a rapid lift recovery as soon as the flow reattachment began (at $\alpha_d \approx 11.4$ deg; Fig. 5) and its return to the unstalled flow values. A detailed analysis of the various unsteady boundary-layer and stall events over an oscillating NACA0012 airfoil is given by Lee and Gerontakos.[19]

The observed increase in the dynamic lift for an oscillating baseline wing was also accompanied by a substantial increase in

nose-down pitching moment (Fig. 4c) and drag force (not shown); a peak value of $C_{m,\text{peak}} = -0.0982$ and $C_{d,\max} = 0.295$, compared to -0.0366 and $C_{d,\text{ss}} = 0.15$ of a static wing at α_{ss}; a 168 and 97% times increase in $-C_{m,\text{peak}}$ and C_d, respectively. The sharp rise in the negative C_m values and the associated negative damping are of particular importance because it results in increased helicopter rotor-blade control loads. On the other hand, in the case of highly maneuverable aircraft, advantage could be made of the increased dynamic lift if the LEV is allowed to form but is delayed in its detachment and shedding from the airfoil suction surface, thereby delaying dynamic stall. Moreover, an $\text{L/D}_{\max}$ of 26 (4.44) was observed during pitch-down at $\alpha_d = 6.13$ deg ($\alpha_{\text{ds}} = 15.15$ deg) for an oscillating baseline wing, compared to $\text{L/D}_{\max} = 23$ (12.9) at $\alpha = 6$ deg (α_{ss}) of a static baseline wing. A dynamic moment stall (corresponding to the angle of attack at which the pitching-moment coefficient started to decrease sharply) at $\alpha_{\text{ms}} = 14.08$ deg, compared to a static $\alpha_{\text{ms}} = 12.5$ deg $= \alpha_{\text{ss}}$, was also observed.

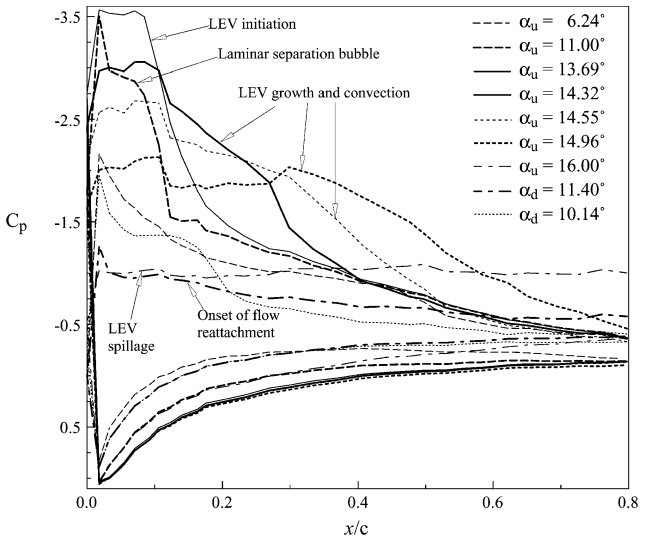

Fig. 5 Pressure distribution shows the presence of a laminar separation bubble and the behavior of a LEV on an oscillating baseline airfoil.

Figure 4a also shows that, similar to the case of a static wing, the addition of a GF increased the effective camber and shifted the dynamic-lift curve vertically upward and that there was a consistent improvement in lift throughout the entire oscillation cycle. A 13 and 26% increase in $C_{l,\max}$, compared to an oscillating baseline wing, was observed for the small and large flaps, respectively. The increase in the dynamic $C_{l,\max}$ was, however, accompanied by an earlier dynamic lift stalling (as a result of the promotion of the LEV formation and spillage) and at the price of an increased $-C_{m,\text{peak}}$ (43 and 64% for $h/c = 1.6$ and 3.2%, respectively). For the 3.2%c GF, a nose-down pitching moment was exhibited over almost the entire oscillation cycle; the 1.6%c GF, however, produced a less severe nose-down pitching moment. The LEV was found to form and detach at $\alpha_{\text{LEV}} = 13.0$ deg (11.63 deg) and $\alpha_{\text{ds}} = 14.87$ deg (13.95 deg) for the 1.6%c (3.2%c) GF, respectively, compared to $\alpha_{\text{LEV}} = 13.69$ deg and $\alpha_{\text{ds}} = 15.15$ deg of a baseline wing. Only a moderate 11% (15%) increase in $C_{d,\max}$, compared to a baseline wing, was observed for the two flaps tested. The presence of a GF also led to an increased $C_{l\alpha}$ (during the first stage of the pitch-up motion or before the formation of the LEV) as a result of a strengthened attached boundary-layer flow and a delayed onset of flow reversal (because of the increase in the suction pressure, as shown in Fig. 6, and the subsequent lessening of the severity of the adverse $\text{d}p/\text{d}x$), compared to a baseline wing, during the pitch-up motion.

The evolution of the C_p distributions of an oscillating airfoil with GF and ITES at selected $\alpha_u = 9.45$, 12.55, and 15.06 deg (during pitch-up) and $\alpha_d = 9.37$ deg (during pitch-down) is displayed in Fig. 6. Figure 6a shows that for the attached flow during the initial stages of pitch-up (i.e., at $\alpha_u = 9.45$ deg), the 3.2%c GF

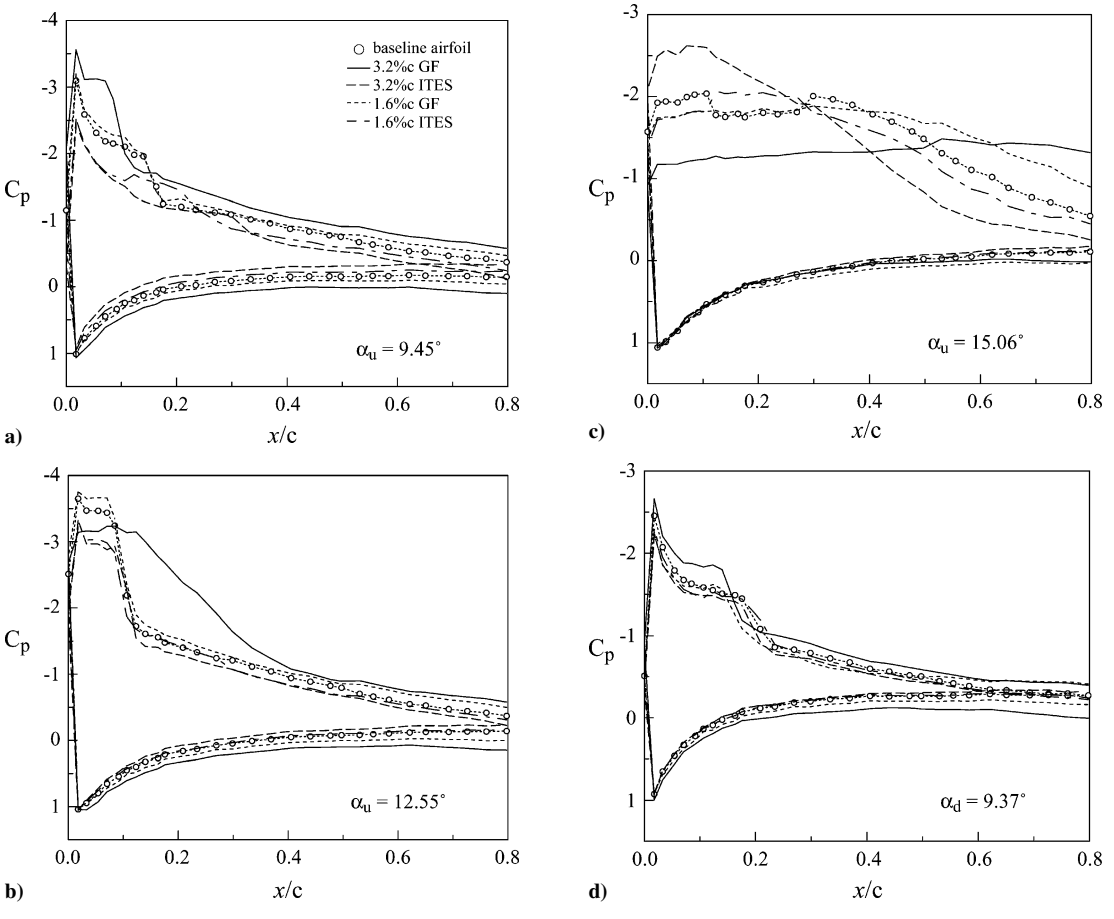

Fig. 6 Effect of trailing-edge strips on oscillating-wing surface-pressure distributions.

Table 2 Variation of critical dynamic aerodynamic performance with trailing-edge strip

Flap configuration	κ	α_{ds}, deg	$C_{l,max}$	$C_{l\alpha}$	$C_{m,peak}$	α_{ms}, deg	$C_{d,max}$	L/D_{max}	α_{or}, deg[a]	L/D_{ds}[b]	α_{LEV}, deg[c]
Baseline wing	0.05	15.15	1.24	0.0662	−0.0982	14.08	0.295	26.0	11.4	4.44	13.69
	0.1	15.85	1.40	0.0701	−0.1181	14.76	0.355	23.6	8.9	4.14	14.08
1.6%c GF	0.05	14.87	1.40	0.0810	−0.1401	13.56	0.328	29.6	10.3	4.60	13.00
	0.1	15.71	1.49	0.0830	−0.1524	14.20	0.375	26.1	8.6	4.10	13.14
3.2%c GF	0.05	13.95	1.56	0.0844	−0.1611	12.40	0.339	27.5	10.6	4.80	11.63
	0.1	15.32	1.72	0.0886	−0.1883	13.42	0.419	27.1	8.8	4.29	12.40
49-deg flap	0.05	14.55	1.48	0.0819	−0.1533	13.14	0.348	23.3	10.6	4.57	12.57
	0.1	15.60	1.67	0.0874	−0.1711	14.08	0.413	23.0	8.5	4.18	13.28
1.6%c ITES	0.05	15.32	1.17	0.0887	−0.0935	14.08	0.290	22.7	10.6	4.12	13.82
	0.1	15.92	1.34	0.0925	−0.1149	14.96	0.340	25.9	8.9	4.11	14.20
3.2%c ITES	0.05	15.54	1.20	0.0993	−0.0962	14.66	0.299	41.6	10.0	4.19	14.32
	0.1	16.00	1.31	0.0963	−0.1190	15.32	0.341	34.3	8.2	3.89	14.76
1.6%c ITES	0.05	14.55	1.54	0.0981	−0.1528	13.14	0.352	28.6	10.3	4.58	12.55
+ 3.2%c GF	0.1	15.60	1.58	0.0927	−0.1548	14.08	0.390	27.9	8.5	4.19	13.14
3.2%c ITES	0.05	15.15	1.32	0.1006	−0.1275	13.95	0.320	25.3	10.3	4.23	13.28
+ 1.6%c GF	0.1	15.89	1.44	0.1001	−0.1497	14.55	0.374	26.4	8.4	3.93	14.07
Inverted 49-deg flap	0.05	15.24	1.21	0.0966	−0.0992	14.08	0.296	24.8	10.9	4.37	13.95
	0.1	15.97	1.32	0.0941	−0.1155	14.96	0.340	24.5	8.8	3.94	14.55

[a] α_{or} = angle of attack at the onset of flow reattachment.
[b] L/D_{ds} = L/D at α_{ds}.
[c] α_{LEV} = angle of attack at the initiation of a LEV.

provided a significant chordwise pressure increase, compared to a baseline wing (denoted by open circle symbols). The increase in the leading-edge suction pressure, including the suction pressure induced by a strengthened laminar separation bubble, was particularly obvious. On the other hand, the majority of the C_p increment provided by the 1.6%c and 49-deg (not shown) flaps was found to be mainly attributed to an increased pressure difference in the aft portion of the airfoil. The promotion in LEV formation for the 3.2%c GF ($\alpha_{LEV} = 11.63$ deg compared to $\alpha_{LEV} = 13.69$ deg of a baseline wing) is evident at $\alpha_u = 12.55$ deg ($> \alpha_{ss}$) given the substantial increase in C_p, especially in the frontal portion of the airfoil, compared to the baseline wing. The LEV detachment or spillage from an oscillating wing with a 3.2%c GF is apparent in Fig. 6c. Figure 6d shows that immediately after the onset of flow reattachment during pitch-down the C_p variation was similar to those described in Fig. 6a but had smaller magnitudes.

The variation of the critical dynamic aerodynamic performance with the Gurney flaps is summarized in Table 2 and Fig. 7. It is clearly seen that the critical values relating to loads increased with the flap height and those relating to incidences were promoted, except for α_{or}. A slightly delayed onset of flow reattachment was observed for a flapped oscillating airfoil, compared to a baseline airfoil. The larger flap ($h/c = 3.2\%$), however, led to an increased degree of asymmetry, or hysteresis, in the dynamic-load loops (caused mainly by the large increase in lift during upstroke), compared to the baseline wing. Figures 4a–4d also indicate that the 49-deg flap provided a C_l-C_m-C_d (C_d not shown) performance (i.e., α_{ds}, $C_{l,max}$, $C_{l\alpha}$, $-C_{m,peak}$, and C_d) in between those of the 1.6%c and 3.2%c GF cases, a phenomenon similar to that observed for a static-wing equipped with a 49-deg flap (Sec. III.A).

The effects of inverted strips (of $h/c = 3.2$ and 1.6%) on the dynamic-load loops at $\kappa = 0.05$ were also examined. As expected, the negative C_p was reduced on the upper surface and increased on the lower surface (in contrast to the regular GF) as shown in Fig. 6. The C_p distributions at low-to-moderate α also display a lowered leading-edge suction peak and a delayed laminar separation bubble (Fig. 6a), compared to a baseline wing with and without GF. At $\alpha_u = 12.55$ deg (Fig. 6b), the behavior of the C_p distribution, especially the leading-edge suction pressure magnitude, was similar to that of a baseline wing but was of lower value, suggesting that the onset of flow reversal was basically unaffected though it reached the leading-edge region later, compared to a baseline wing as well as the wing with GF, thus leading to an increased $C_{l\alpha}$ (Fig. 4a). In the meantime, the formation (at $\alpha_{LEV} = 13.82$ and 14.32 deg for the 1.6%c and 3.2%c ITES, respectively) and detachment of a LEV was delayed (Figs. 6c and 6d), which resulted in a delayed dynamic stall with a lowered $C_{l,max}$ (Table 2). Note that the effective negative

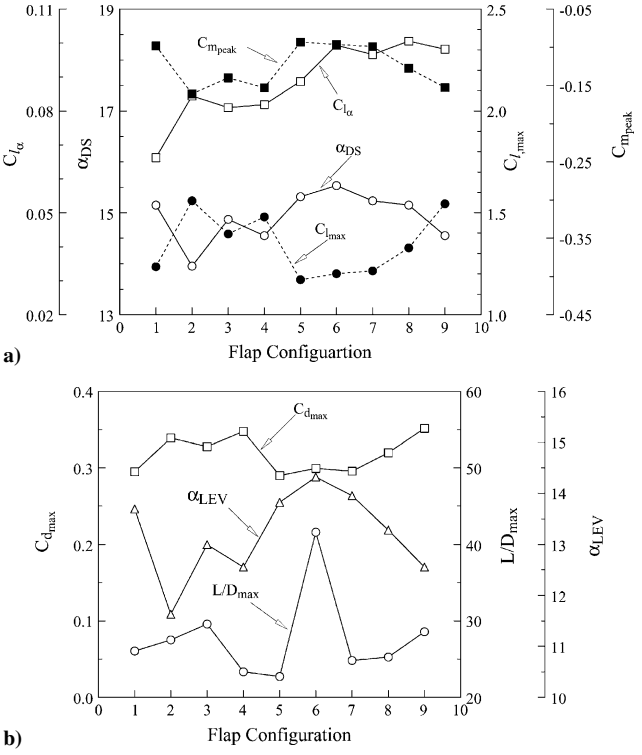

Fig. 7 Variation of critical dynamic aerodynamic performance with trailing-edge strip. Flap configurations: ①, baseline airfoil; ②, 3.2%c Gurney flap; ③, 1.6%c Gurney flap; ④, 49-deg flap; ⑤, 1.6%c ITES; ⑥, 3.2%c ITES; ⑦, inverted 49-deg flap; ⑧, 3.2%c ITES and 1.6%c Gurney flap; and ⑨, 1.6%c ITES and 3.2%c Gurney flap.

camber induced by the inverted flaps also led to an alleviated nose-down pitching-moment tendency. The airfoil incidence at which the flow reattachment began remained virtually the same, compared with the GF case, though at lower C_p magnitudes than the baseline wing (Fig. 6d).

The C_l-C_m-C_d loops (Figs. 4a and 4c; C_d not shown) also indicate that, in contrast to the GF, the asymmetry in hysteresis was reduced with increasing ITES height, attributing to the decrease in lift during pitch-up and the largely unaffected lift performance during the pitch-down flow process. Note that the oscillating wing experienced no effect of the presence of the inverted flaps during downstroke (because the flaps were located inside of a completely separated flow

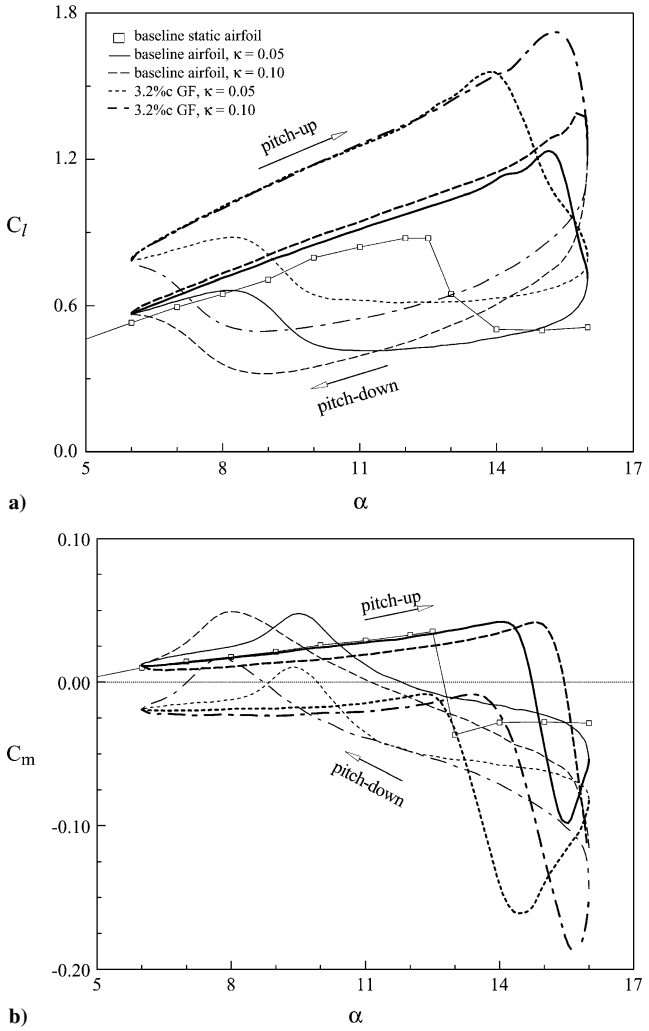

Fig. 8 Typical variation of dynamic-load loops with reduced frequency.

from the upper surface of the airfoil), and, therefore, resulted in a small variation in C_d and C_m, especially for the inverted 1.6%c and 49-deg flaps, during the poststall flow conditions. A substantial reduction in the negative C_m values throughout the entire oscillation was observed, compared to the regular Gurney flaps. Similar to the Gurney flaps, the values of $\alpha_{\rm ds}$, $C_{l,\max}$, $C_{l\alpha}$, and $-C_{m,\rm peak}$ increased with the height of the ITES (Table 2). The $C_{d,\max}$ values were lower than the wing with Gurney flaps and were found to decrease slightly with decreasing ITES flap height. No significant variation in $\rm L/D_{max}$ existed for an oscillating wing with and without flaps except for the 3.2%c ITES case, which gave a large increase in $\rm L/D_{max}$. The 3.2%c ITES also produced the highest values of $\alpha_{\rm ds}$, $C_{l\alpha}$, and $\rm L/D_{max}$ with low values in $C_{l,\max}$, $C_{d,\max}$, and $-C_{m,\rm peak}$ among the eight flap configurations tested (Table 2 and Fig. 7).

The possibility of the control of both the detrimental hysteresis in lift and the accompanied nose-down pitching moment, as well as the desirable increase in $\alpha_{\rm ds}$, $C_{l,\max}$, and $C_{l\alpha}$ of an unsteady airfoil via regular GF or ITES can be also reflected from the application of the asymmetric strips. The 3.2%c/1.6%c asymmetric strip provided a compromise, in terms of $\alpha_{\rm ds}$, $C_{l,\max}$, $-C_{m,\rm peak}$, and $C_{d,\max}$ (Figs. 4b, 4d, and 7 and Table 2) and C_p and $\alpha_{\rm LEV}$ behavior (Fig. 6), between a 3.2%c ITES and a 1.6%c GF, while the lift-curve slope remained about the same as a 3.2%c ITES and $\rm L/D_{max}$ was near the value of the 1.6%c GF. Similar to the 3.2%c/1.6%c strip configuration, the 1.6%c/3.2%c configuration also provided an improvement, or compromise, between a 1.6%c ITES and a 3.2%c GF. The 1.6%c/3.2%c asymmetric strip, however, promoted the dynamic lift stalling with a larger increase in $C_{l,\max}$, compared to the 3.2%c/1.6%c strip, at the price of a further increase in the drag and $-C_{m,\rm peak}$. Also, for an inverted 49-deg flap, the overall aerodynamic performance was found to be in between those of the 1.6%c and 3.2%c ITES cases. In summary, the addition of passive Gurney flaps or ITES to an oscillating wing should provide another look into the control of rotorcraft retreating-blade dynamic stall and also the blade-vortex interaction via the upward and downward deflections of a movable trailing-edge flap.

Finally, the effects of reduced frequency on the dynamic-load loops with and without flaps were also investigated for $\kappa = 0.1$ and are summarized in Fig. 8. The dynamic-stall events were found to occur at successively later times as κ was increased, that is, the formation and rearward convection of the LEV was delayed to higher α with increasing κ (Table 2). The increase in $\alpha_{\rm ds}$ and $C_{l,\max}$ was, however, more obvious at higher κ (Fig. 8a), and the continuous drop in C_l observed during the poststall condition became less significant. The improvement in $\alpha_{\rm ds}$, $C_{l,\max}$, and $C_{l\alpha}$ was found to be accompanied by an increase in $-C_{m,\rm peak}$ (Fig. 8b) and $C_{d,\max}$. The reattachment process was, however, further delayed with increasing κ. Table 2 shows that a systematical increase in the critical values of $\alpha_{\rm ds}$, $C_{l,\max}$, $-C_{m,\rm peak}$, $\alpha_{\rm ms}$, and $C_{d,\max}$ (however not in $C_{l\alpha}$) of an oscillating wing with and without flaps at $\kappa = 0.1$ was observed, compared to $\kappa = 0.05$.

IV. Conclusions

The dynamic-load loops of an oscillating NACA 0012 airfoil with and without small trailing-edge flaps were characterized at $Re = 1.07 \times 10^5$. The flapped static-wing configurations were also included for comparison. The results show that on the basis of the eight flap configurations tested it appears that, similar to a static wing, the Gurney flap concept (including the 49-deg flap) was also fairly generally applicable for an oscillating airfoil in terms of $C_{l,\max}$, $C_{l\alpha}$, and lift increment except for the large (small) increase in $-C_{m,\rm peak}$ ($C_{d,\max}$) accompanied by a promoted dynamic stall. The increase (decrease) in the nose-down C_m ($\alpha_{\rm ds}$) could be alleviated by the use of inverted strips at the price of a reduced $C_{l,\max}$. The asymmetric strips were found to provide a compromise in the dynamic aerodynamic performance and the detrimental hysteresis between the regular and inverted Gurney flaps. Both the static- and dynamic-stall mechanisms were basically unchanged compared to a baseline airfoil. The present passive dynamic stall and pitching moment control can be valuable because they can be used as an experimental guideline for the active control of the dynamic stall and/or nose-down pitching moment via the use of a spanwise trailing-edge flap. Detailed knowledge of the flowfield (performed at much higher Reynolds numbers), including the loadings in the trailing-edge region, however, is needed so as to better quantify the findings reported here.

Acknowledgment

This work was supported by the Natural Science and Engineering Research Council (NSERC) of Canada.

References

[1]Liebeck, R. H., "Design of Subsonic Airfoils for High Lift," *Journal of Aircraft*, Vol. 15, No. 9, 1978, pp. 547–561.

[2]Roesch, P., and Vuillet, A., "New Designs for Improved Aerodynamic Stability on Recent Aerospatiale Helicopters," *Vertica*, Vol. 6, Jan. 1982, pp. 145–164.

[3]Neuhart, D. H., and Pendergraft, O. C., "A Water Tunnel Study of Gurney Flaps," NASA TM 4071, Nov. 1988.

[4]Katz, J., and Largman, R., "Effect of 90 Degree Flap on the Aerodynamics of a Two-Element Airfoil," *Journal of Fluids Engineering*, Vol. 111, March 1989, pp. 93, 94.

[5]Storms, B. L., and Jang, C. S., "Lift Enhancement of an Airfoil Using a Gurney Flap and Vortex Generators," *Journal of Aircraft*, Vol. 31, No. 3, 1994, pp. 542–547.

[6]Kentfield, J. A. C., and Clavelle, E. J., "The Flow Physics of Gurney Flaps, Devices for Improving Turbine Blade Performance," *Wind Engineering*, Vol. 17, No. 1, 1993, pp. 24–34.

[7]Ross, J. C., Storms, B. L., and Carrannanto, P. G., "Lift-Enhancing Tabs on Multielement Airfoil," *Journal of Aircraft*, Vol. 32, No. 5, 1995, pp. 1072–1078.

[8]Bloy, A. W., and Durrant, M. T., "Aerodynamic Characteristics of an Aerofoil with Small Trailing Edge Flaps," *Wind Engineering*, Vol. 19, No. 3, 1995, pp. 167–172.

[9]Myose, R., Papadakis, M., and Heron, I., "Gurney Flap Experiments on Airfoils, Wings, and Reflection Plane Model," *Journal of Aircraft*, Vol. 35, No. 2, 1998, pp. 206–211.

[10]van Dam, C. P., Yen, D. T., and Vijgen, P. M. H. W., "Gurney Flap Experiments on Airfoil and Wings," *Journal of Aircraft*, Vol. 36, No. 2, 1999, pp. 484–486.

[11]Jeffrey, D., Zhang, X., and Hurst, D. W., "Aerodynamics of Gurney Flaps on a Single-Element High-Lift Wing," *Journal of Aircraft*, Vol. 37, No. 2, 2000, pp. 295–301.

[12]Li, Y., Wang, J., and Zhang, P., "Effects of Gurney Flaps on a NACA 0012 Airfoil," *Flow, Turbulence and Combustion*, Vol. 68, No. 1, 2002, pp. 27–39.

[13]Zhan, J. X., and Wang, J. J., "Experimental Study of Gurney Flap and Apex Flap on a Delta Wing," *Journal of Aircraft*, Vol. 41, No. 6, 2004, pp. 1379–1383.

[14]Gai, S. L., and Palfrey, R., "Influence of Trailing-Edge Flow Control on Airfoil Performance," *Journal of Aircraft*, Vol. 40, No. 2, 2003, pp. 332–337.

[15]McCroskey, W. J., McAlister, K. W., Carr, L. W., Pucci, S. L., Lamber, O., and Indergrand, R. F., "Dynamic Stall on Advanced Airfoil Sections," *Journal of American Helicopter Society*, Vol. 26, July 1981, pp. 40–50.

[16]McCroskey, W. J., "Unsteady Airfoils," *Annual Review of Fluid Mechanics*, Vol. 14, 1982, pp. 285–311.

[17]Ericsson, L. E., and Reding, J. P., "Fluid Mechanics of Dynamic Stall. Part I. Unsteady Flow Concepts," *Journal of Fluids and Structures*, Vol. 2, Jan. 1988, pp. 1–33.

[18]Lee, T., and Basu, S., "Measurement of Unsteady Boundary Layer Developed on an Oscillating Airfoil Using Multiple Hot-Film Sensors," *Experiments in Fluids*, Vol. 25, No. 2, 1998, pp. 108–117.

[19]Lee, T., and Gerontakos, P., "Investigation of Flow over an Oscillating Airfoil," *Journal of Fluid Mechanics*, Vol. 512, 2004, pp. 313–341.

[20]Rennie, R. M., and Jumper, E. J., "Experimental Measurements of Dynamic Control Surface Effectiveness," *Journal of Aircraft*, Vol. 33, No. 5, 1996, pp. 880–887.

[21]Smith, A. M. O., "High-Lift Aerodynamics," *Journal of Aircraft*, Vol. 12, No. 6, 1975, pp. 501–530.